Acta Crystallographica Section D
Biological Crystallography
ISSN 0907-4449

Structure and substrate docking of a hydroxy(phenyl)pyruvate reductase from the higher plant *Coleus blumei* Benth.

Verena Janiak,[a] Maike Petersen,[a] Matthias Zentgraf,[b] Gerhard Klebe[b] and Andreas Heine[b]*

[a]Institut für Pharmazeutische Biologie, Philipps-Universität Marburg, Deutschhausstrasse 17A, 35037 Marburg, Germany, and [b]Institut für Pharmazeutische Chemie, Philipps-Universität Marburg, Marbacher Weg 6, 35032 Marburg, Germany

Correspondence e-mail: heinea@mailer.uni-marburg.de

Received 22 December 2009
Accepted 18 February 2010

PDB References:
hydroxy(phenyl)pyruvate reductase, apo form, 3ba1; holo form, 3baz.

Hydroxy(phenyl)pyruvate reductase [H(P)PR] belongs to the family of D-isomer-specific 2-hydroxyacid dehydrogenases and catalyzes the reduction of hydroxyphenylpyruvates as well as hydroxypyruvate and pyruvate to the corresponding lactates. Other non-aromatic substrates are also accepted. NADPH is the preferred cosubstrate. The crystal structure of the enzyme from *Coleus blumei* (Lamiaceae) has been determined at 1.47 Å resolution. In addition to the apoenzyme, the structure of a complex with $NADP^+$ was determined at a resolution of 2.2 Å. H(P)PR is a dimer with a molecular mass of 34 113 Da per subunit. The structure is similar to those of other members of the enzyme family and consists of two domains separated by a deep catalytic cleft. To gain insights into substrate binding, several compounds were docked into the cosubstrate complex structure using the program *AutoDock*. The results show two possible binding modes with similar docking energy. However, only binding mode *A* provides the necessary environment in the active centre for hydride and proton transfer during reduction, leading to the formation of the (*R*)-enantiomer of lactate and/or hydroxyphenyllactate.

1. Introduction

While searching for enzymes that are involved in the biosynthesis of rosmarinic acid (RA) in *Coleus blumei* Benth. (synonym *Solenostemon scutellarioides*, Lamiaceae), we purified an enzyme that reduces 4-hydroxyphenylpyruvate (pHPP) to 4-hydroxyphenyllactate, the direct precursor needed for ester formation in the biosynthesis of rosmarinic acid, and cloned the corresponding cDNA (EMBL accession No. AJ507733; Petersen *et al.*, 1993; Kim *et al.*, 2004). The nucleotide and amino-acid sequences revealed that this enzyme, hydroxyphenylpyruvate reductase (HPPR; EC 1.1.1.237), belongs to the family of D-isomer-specific 2-hydroxyacid dehydrogenases (Grant, 1989). In RA biosynthesis, HPPR catalyzes the NAD(P)H-dependent reduction of 4-hydroxyphenylpyruvate to 4-hydroxyphenyllactate (Fig. 1). The reverse oxidation reaction is also catalyzed by the enzyme *in vitro*. The enzyme was characterized in cell-free extracts from suspension-cultured cells of *C. blumei* (Petersen & Alfermann, 1988; Häusler *et al.*, 1991). In addition to 4-hydroxyphenylpyruvate, 3,4-dihydroxyphenylpyruvate (DHPP) is accepted as substrate by the native enzyme although with lower affinity. NADH as well as NADPH can serve as the electron donor.

The putative HPPR cDNA was heterologously expressed in *Escherichia coli* with an N-terminal His tag and the expected

enzyme activities were demonstrated (Kim *et al.*, 2004). The heterologously expressed protein showed a preference for hydroxypyruvate (HP) over 4-hydroxyphenylpyruvate as substrate and is therefore presented as hydroxy(phenyl)pyruvate reductase [H(P)PR] in this paper (V. Janiak, PhD thesis). The H(P)PR monomer from *C. blumei* consists of 313 amino-acid residues with a calculated mass of 34 113 Da. Similar cDNA sequences with previously unknown functions were found in *Salvia miltiorrhiza* (EMBL DQ099741, 87.7% identity on a nucleotide basis, Lamiaceae), *Lycopersicon esculentum* (EMBL BT013950, 72.9% identity, Solanaceae), *Lotus corniculatus* var. *japo* (EMBL AP006863, 69.9% identity, Fabaceae) and *Arabidopsis thaliana* (EMBL AAL47452, AAG52259, AAM65710, AAM47330, 68.2% identity, Brassicaceae). Only the genus *Salvia* is known to accumulate RA. Recently, the orthologous gene from *Arabidopis thaliana* was shown to encode a cytosolic hydroxypyruvate reductase (HPR2) that is involved in photorespiration (Timm *et al.*, 2008).

Generally, D-isomer-specific 2-hydroxyacid dehydrogenases catalyze the reduction of 2-oxoacids to the D-isomers of the respective 2-hydroxyacids or the corresponding reverse oxidation reaction. Well known enzymes of this class include D-lactate dehydrogenase, D-glycerate dehydrogenase, D-3-phosphoglycerate dehydrogenase and D-2-hydroxyisocaproate dehydrogenase, all of which occur in prokaryotic organisms. Enzymes of this class with a broad substrate specificity have even been described from archaea (Bonete *et al.*, 2000). NADH-dependent peroxisomal D-hydroxypyruvate reductase has been described as being involved in photorespiration in higher plants, *e.g. Cucumis sativus* (Greenler *et al.*, 1989). NADH mostly serves as the electron donor; only a few members of this family have been shown to accept NADPH as the preferred cosubstrate, *e.g.* 2-ketoaldonate reductases from *E. coli* (Yum *et al.*, 1998; Nunez *et al.*, 2001), the VanH protein, involved in vancomycin resistance, from *Enterococcus faecium* (Bugg *et al.*, 1991) and human glyoxylate reductase/hydroxypyruvate reductase (Booth *et al.*, 2006).

Hydroxypyruvate reductases (HPRs) in higher plants exist as NADH-dependent peroxisomal enzymes (EC 1.1.1.29) and NAD(P)H-dependent cytosolic enzymes (EC 1.1.1.81) (Greenler *et al.*, 1989; Julliard & Breton-Gilet, 1997; Kleczkowski *et al.*, 1988). cDNA sequences for both HPR and H(P)PR from *C. blumei* have recently been deposited (EMBL AJ507733 and EF125078). Both proteins belong to the family of D-isomer-specific 2-hydroxyacid dehydrogenases, but share a low sequence similarity of only ∼25%.

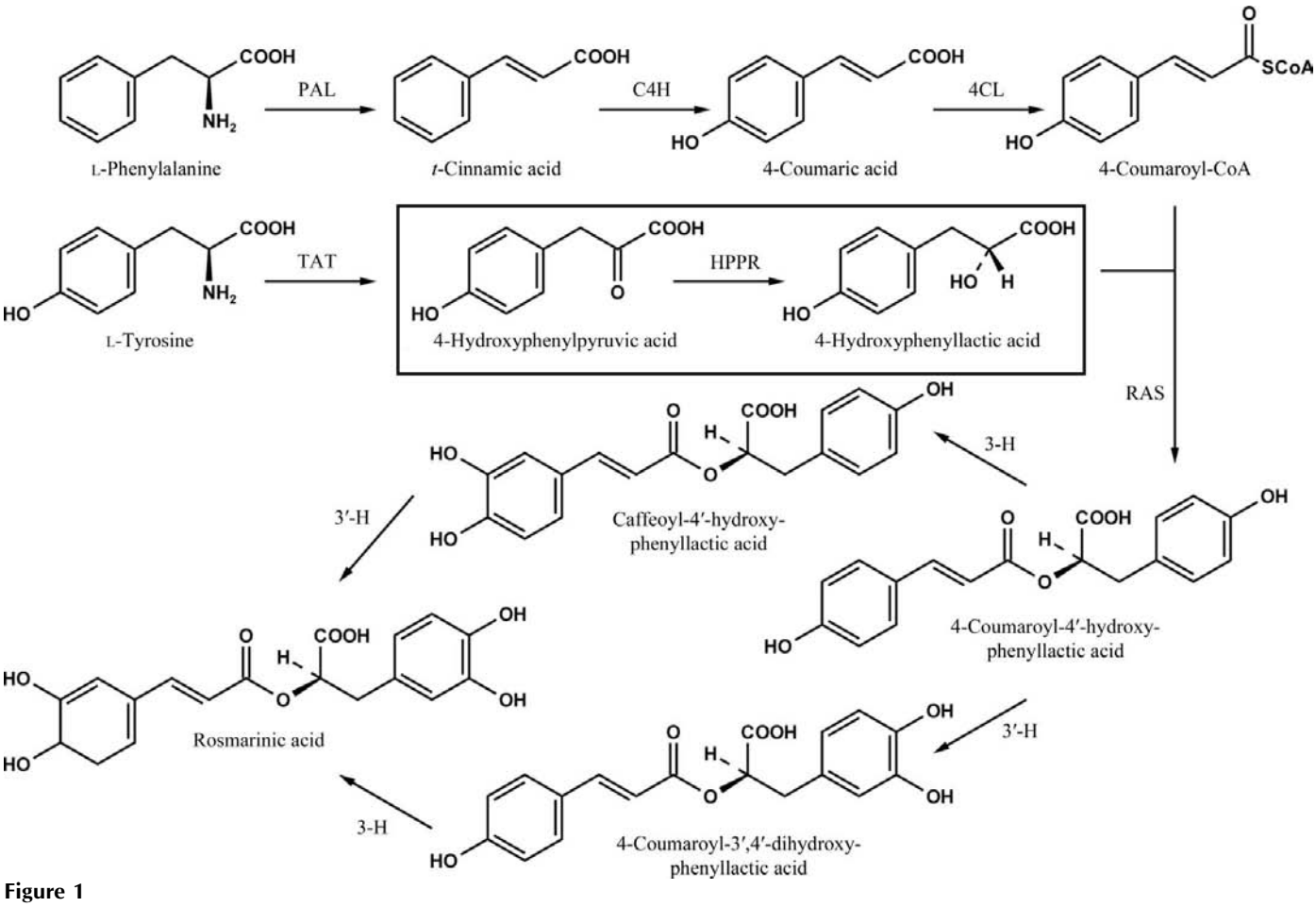

Figure 1
Pathway of rosmarinic acid biosynthesis in *C. blumei*. PAL, phenylalanine ammonia-lyase; C4H, cinnamic acid 4-hydroxylase; 4CL, hydroxycinnamic acid:CoA ligase; TAT, tyrosine aminotransferase; HPPR, hydroxyphenylpyruvate reductase; RAS, rosmarinic acid synthase; 3-H, hydroxycinnamoyl-hydroxyphenyllactate 3-hydroxylase; 3′-H, hydroxycinnamoyl-hydroxyphenyllactate 3′-hydroxylase.

Several crystal structures of prokaryotic D-isomer-specific 2-hydroxyacid dehydrogenases have been published, *e.g.* those of D-glycerate dehydrogenase (GDH) from *Hyphomicrobium methylovorum* (PDB code 1gdh; Goldberg *et al.*, 1994), formate dehydrogenase from *Pseudomonas* sp. (PDB codes 2nac and 2nad; Lamzin *et al.*, 1994), D-3-phosphoglycerate dehydrogenase (PGDH) from *E. coli* (PDB code 1psd; Schuller *et al.*, 1995), D-lactate dehydrogenase from *Lactobacillus bulgaricus* (Nessler *et al.*, 1994) and *L. pentosus* and D-hydroxyisocaproate dehydrogenase from *L. casei* (PDB code 1dxy; Dengler *et al.*, 1997). These enzymes are mostly active as dimers apart, for example, from D-3-phosphoglycerate dehydrogenase from *E. coli*, which is a tetramer (Schuller *et al.*, 1995). The latter enzyme also differs from the general structure by the presence of an additional regulatory domain in addition to the two domains that are present in all known enzymes: the cosubstrate-binding domain and the substrate-binding domain. The cosubstrate-binding domain carries the conserved sequence motif -G-*X*-G-*X*-*X*-G- (where *X* can be any amino acid). This NAD(P)/NAD(P)H-binding domain also occurs in L-2-hydroxyacid dehydrogenases, which are not otherwise evolutionarily related to the D-isomer-specific class of 2-hydroxyacid dehydrogenases (Stoll *et al.*, 1996).

Here, we describe the crystal structure determination at 1.47 Å resolution of a D-isomer-specific 2-hydroxyacid dehydrogenase from the higher plant *C. blumei* (Lamiaceae) which accepts large substrates such as 4-hydroxyphenylpyruvate and 3,4-dihydroxyphenylpyruvate as well as smaller molecules and prefers NADPH as cosubstrate (Fig. 2). Additionally, we determined the crystal structure of a complex with the cosubstrate $NADP^+$, which serves as a template for substrate docking with the program *AutoDock* (Morris *et al.*, 1998). Various substrates were docked into the enzyme active site to detect possible binding modes.

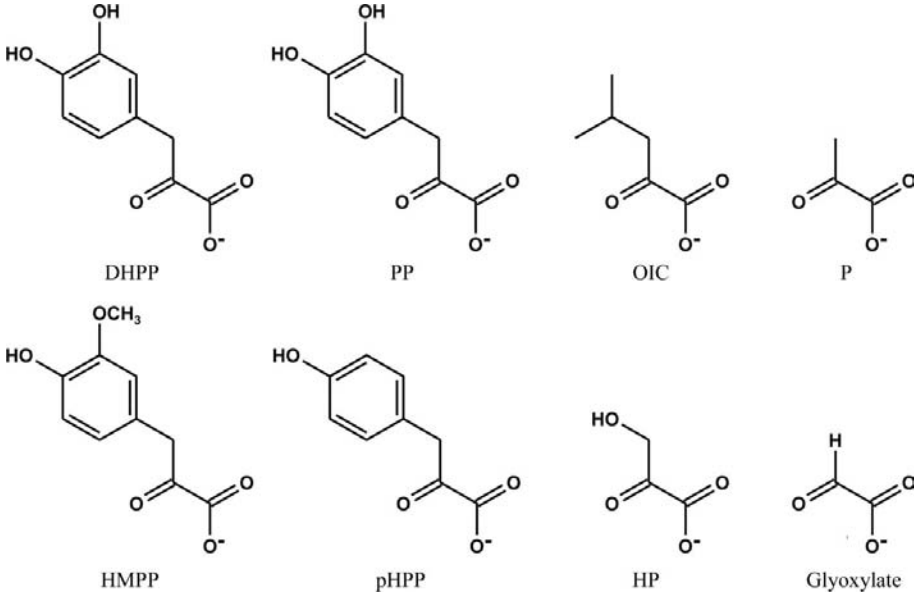

Figure 2
In addition to 4-hydroxyphenylpyruvate (pHPP), H(P)PR accepts the following compounds as substrates: 3,4-dihydroxyphenylpyruvate (DHPP), phenylpyruvate (PP), pyruvate (P), glyoxylate, 4-hydroxy-3-methoxyphenylpyruvate (HMP), hydroxypyruvate (HP) and 2-oxoisocaproate (OIC).

2. Experimental

2.1. Enzyme preparation and crystallization

Cloning of the putative H(P)PR cDNA in pET-15b (Novagen), expression in *E. coli* BL21 (DE3) pLysS (Novagen) and protein isolation have been described by Petersen *et al.* (1993) and Kim *et al.* (2004). The His-tagged H(P)PR protein was purified using an Ni–NTA His-Bind column (Qiagen) according to the manufacturer's protocol. After a buffer change to 10 m*M* potassium phosphate pH 6.5 by passage over a PD-10 desalting column (GE Healthcare), the protein was loaded onto a 2′,5′-ADP-Sepharose 4B column (GE Healthcare) pre-equilibrated with buffer *A* [10 m*M* potassium phosphate pH 6.5, 1 m*M* dithiothreitol (DTT)]. After washing with 16 ml buffer *A*, the bound protein was eluted with a linear NaCl gradient (0–1 *M*). The fractions showing HPPR activity were pooled, concentrated by centrifugation using Ultrafree-15 units (Biomax) to a protein concentration of ∼6 mg ml^{-1} and dialyzed against 50 m*M* Tris–HCl pH 7.0.

Crystallization was performed by the sitting-drop vapour-diffusion method. The droplets were prepared by mixing 1 µl well solution with an equal amount of protein solution. Different crystallization conditions were tested and led to a variety of crystal shapes. One crystal cluster was obtained after several days in 30% 2-methyl-2,4-pentanediol (MPD), 0.2 *M* NaCl, 0.1 *M* Tris–HCl pH 7.5 at 277 K and one fragment from the cluster was used for data collection. H(P)PR crystallized in space group $P3_121$, with unit-cell parameters $a = b = 62.9$, $c = 153.3$ Å. Owing to the presence of MPD no further cryoprotection was needed for low-temperature data collection.

Tetragonal bipyramid-shaped crystals of the complex were obtained using Ni–NTA-purified protein (15 mg ml^{-1} protein, 2 m*M* $NADP^+$) in a solution consisting of 20% polyethylene glycol (PEG) 1000, 0.1 *M* imidazole pH 7.5, 4 m*M* 4-hydroxyphenylpyruvate (pHPP), 0.2 m*M* DTT at 299 K. The crystals grew in space group $P4_12_12$, with unit-cell parameters $a = b = 63.5$, $c = 222.6$ Å. 20% glycerol was used as a cryoprotectant for low-temperature data collection.

2.2. Data collection

Data were collected at 100 K on beamline PSF1 at the BESSY II synchrotron, Berlin. The crystal was exposed for 5 s at a wavelength of 0.91838 Å and the diffraction pattern was recorded on a MAR CCD detector. A data set for the $NADP^+$ complex was collected on a Rigaku copper rotating-anode generator operating at 50 keV and 90 mA using an R-AXIS IV image-plate detector. Here, the exposure was 12 min with a rotation of $\Delta\varphi = 0.5^\circ$. All data were processed and scaled with the programs *DENZO* and *SCALEPACK*

Table 1
Data-collection and refinement statistics.

Values in parentheses are for the highest resolution shell.

	H(P)PR	$NADP^+$ complex
Data collection and processing		
Wavelength (Å)	0.91838	1.5418
Space group	$P3_121$	$P4_12_12$
Unit-cell parameters (Å)	$a = b = 62.9$, $c = 153.3$	$a = b = 63.5$, $c = 222.6$
Resolution range (Å)	50.0–1.47 (1.50–1.47)	30.0–2.20 (2.25–2.20)
Wilson B factor (Å^2)	20.5	31.8
No. of observations	339466	293424
Unique reflections	58971	23761
$R_{\rm merge}$† (%)	7.0 (46.6)	9.9 (55.9)
Completeness (%)	96.9 (99.1)	98.1 (81.4)
$\langle I/\sigma(I)\rangle$	23.9 (3.4)	24.3 (2.6)
Refinement		
Resolution range (Å)	10–1.47	10.0–2.20
$R_{\rm cryst}$‡ (%)		
$F_{\rm o} > 4\sigma(F_{\rm o})$	14.1	19.2
All $F_{\rm o}$	14.9	21.1
$R_{\rm free}$§ (%)		
$F_{\rm o} > 4\sigma(F_{\rm o})$	19.3	23.5
All $F_{\rm o}$	20.3	26.0
Refined residues	312	311
Water molecules	290	144
Ligand atoms	—	48
R.m.s.d. bond angles (°)	2.3	1.8
R.m.s.d. bond distances (Å)	0.012	0.007
Ramachandran plot		
Most favoured regions (%)	90.2	88.3
Additionally allowed regions (%)	9.4	11.3
Generously allowed regions (%)	0.0	0.0
Disallowed (%)	0.4	0.4
Mean B factors (Å^2)		
Protein non-H atoms	23.6	30.1
Main chain (Å^2)	21.0	29.0
Side chain (Å^2)	26.4	31.2
Water molecules	34.6	35.4
Ligand atoms	—	29.6
PDB code	3ba1	3baz

† $R_{\rm merge} = \sum_{hkl}\sum_i |I_i(hkl) - \langle I(hkl)\rangle| / \sum_{hkl}\sum_i I_i(hkl)$, where $\langle I(hkl)\rangle$ is the mean of the i observations of reflection hkl. ‡ $R_{\rm cryst} = \sum_{hkl} ||F_{\rm obs}| - |F_{\rm calc}|| / \sum_{hkl} |F_{\rm obs}|$. § $R_{\rm free}$ is calculated in the same manner as $R_{\rm cryst}$ but from 5% of the data that were not used for refinement.

as implemented in the *HKL*-2000 package (Otwinowski & Minor, 1997) to resolutions of 1.47 and 2.2 Å for the apo and holo forms, respectively. Further data-collection statistics are summarized in Table 1.

2.3. Structure solution and refinement

Structure solution was attempted by using the molecular-replacement method with the programs *AMoRe* (Navaza, 1994), *MOLREP* (Vagin & Teplyakov, 1997) and *Beast* (Read, 2001) as implemented in the *CCP*4 suite (Collaborative Computational Project, Number 4, 1994). Various computer-generated homology models were tried as search models. Unfortunately, none of the models or programs resulted in a unique solution of the rotation and translation functions. Therefore, an additional model was automatically generated using the *SWISS-MODEL* server (Schwede *et al.*, 2003). This model consisted of the following oxidoreductases: glycerate dehydrogenase (PDB code 1gdh; UniProtKB P36234; Goldberg *et al.*, 1994), D-3-phosphoglycerate dehydrogenase (PDB code 1psd; UniProtKB P0A9T0; Schuller *et al.*, 1995) and NAD-dependent formate dehydrogenase (PDB code 2nad; UniProtKB P33160; Lamzin *et al.*, 1994). These proteins had a sequence identity of 23–31% and a sequence similarity of 35–51% to the amino-acid sequence of H(P)PR. Using the molecular-replacement program *Phaser* (McCoy *et al.*, 2005; resolution range 10.0–4 Å), a potential solution with a log-likelihood gain of 28.3 was obtained. Visual inspection of the calculated electron density within the program *O* (Jones *et al.*, 1991) showed promising areas of connected density for parts of the molecule. 95 of 313 residues showed consistent electron density and these residues were used as a starting model for phase extension and model optimization in *ARP*/*wARP* (Lamzin & Wilson, 1993). This homology model, together with a comparison with the final structure, is visualized in Figs. 5(*b*) and 5(*c*). Iterative cycles of refinement and electron-density calculation resulted in an almost complete model consisting of 298 residues in five polypeptide chains with a connectivity index of 0.97. This model was further refined in *CNS* (Brünger *et al.*, 1998) using rigid-body, positional and slow-cooling refinement protocols. At later stages, the program *SHELXL* (Sheldrick, 2008) was used for conjugate-gradient refinement with default restraints on bonding geometry and B values. Intermittent cycles of manual model building were performed in *O* (Jones *et al.*, 1991). During the last refinement, H atoms were added using a riding model without the use of any additional parameters. The low-resolution cutoff was also set to 10 Å at this point owing to insufficient diffuse solvent correction using Babinet's principle (Moews & Kretsinger, 1975) as implemented in *SHELXL*. 5% of all data were used for $R_{\rm free}$ calculation. The final model contained 312 amino acids and 290 water molecules. Since the space group changed to $P4_12_12$ for the complex structure, molecular replacement was repeated with the previously refined structure using the program *Phaser* (McCoy *et al.*, 2005). Clear density for the cosubstrate was visible in $\sigma_{\rm A}$-weighted $2F_{\rm o} - F_{\rm c}$ and $F_{\rm o} - F_{\rm c}$ maps upon inspection in *O* (Jones *et al.*, 1991). The cosubstrate was constructed and minimized in *SYBYL* (*SYBYL* Molecular Modeling Software, v.7.0; Tripos Inc., St Louis, Missouri, USA) and added to the model for further refinement. In both structures, residue Asp98 is in a disallowed region of the Ramachandran plot but shows clear electron density and is located at a tip of a γ turn, as commonly observed in other protein structures (Arévalo *et al.*, 1993). Final refinement statistics are given in Table 1.

2.4. Docking

All substrates were constructed and minimized using the program *SYBYL*. Partial charges were assigned to the substrate atoms and the $NADP^+$ cosubstrate according to Gasteiger & Marsili (1980). The number of rotatable torsion angles was set by *AutoTors* and the ligands were docked within a search area defined by a grid of $20 \times 22 \times 24$ Å with a spacing of 0.5 Å encompassing the active-site cleft. Polar H atoms, charges and solvation parameters were added to the

protein coordinate file with 'protonate' and 'add_chrgsol', which is a modified version of the ADDSOL utility in *AutoDock* 3.0 with charges from the united-atom model of AMBER (Case *et al.*, 2006). *AutoDock* 3.0 was used for flexible ligand docking using the implemented Lamarckian genetic algorithm (Morris *et al.*, 1998), applying a standard setup with an initial population of 50 random placed individuals, a maximum of 3×10^6 energy evaluations, a mutation range of 0.02, a crossover rate of 0.80 and an elitism value of 1.0 for each run. 100 independent docking runs were carried out for each ligand and ranked according to their mean docking energy by the scoring function of *AutoDock*. Results that differed by less than 1.0 Å in positional root-mean square deviation (r.m.s.d.) were clustered and represented by the result with the most favourable free energy of binding.

2.5. Analysis of the H(P)PR reaction product

The reaction product of H(P)PR from standard assays using 4-hydroxyphenylpyruvate and NADPH as substrates was extracted with ethyl acetate and purified by thin-layer chromatography on silica-gel 60 F_{254} plates with 63:10:27 *n*-butanol:acetic acid:H_2O as the mobile phase together with 4-hydroxyphenyllactate (pHPL) as the reference. The band corresponding to pHPL was scraped off the plate and eluted twice with 1 ml methanol. The eluate was re-chromatographed with the same system and eluted again. Chiral HPLC was performed with a Eurocel 01 column (250 × 4.6 mm, 5 µm; Knauer) using 90:10 *n*-hexane:2-propanol with 0.1% trifluoroacetic acid as the mobile phase at a flow rate of 1.5 ml min^{-1}. Eluted substances were detected at 280 nm. Racemic pHPL and (*S*)-pHPL (= L-pHPL; Interchim) were used as references.

3. Results and discussion

3.1. Overall structure

The structure of H(P)PR shows the typical topology of members of the D-isomer-specific 2-hydroxyacid dehydrogenase family, with two domains separated by a deep cleft that contains the active site (Fig. 3). The exceptions are phosphoglycerate dehydrogenase and erythronate-4-phosphate dehy-

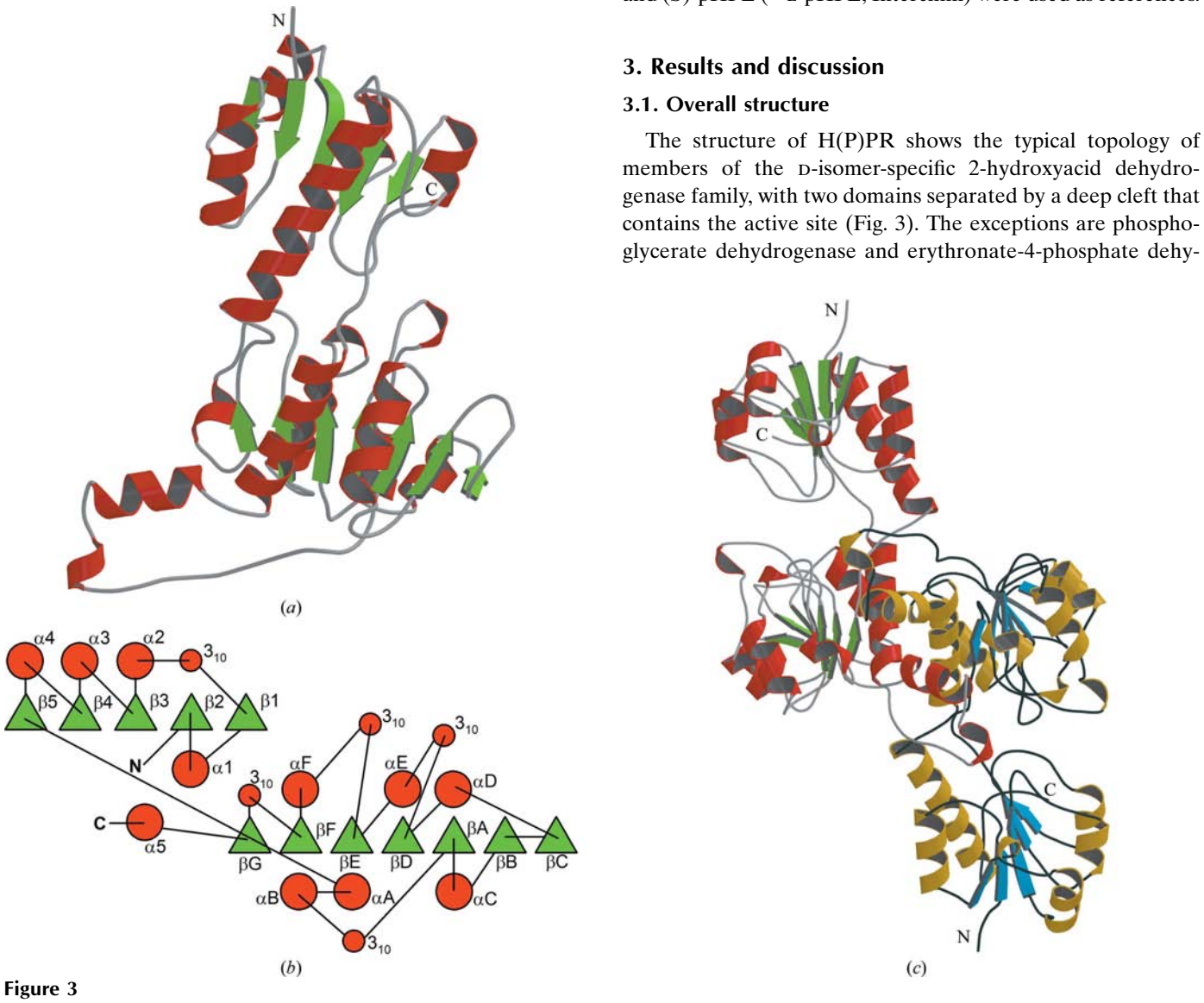

Figure 3
(*a*) Ribbon diagram of H(P)PR generated from the refined crystal structure. The monomer located in the asymmetric unit is depicted. Secondary-structure elements were assigned with the program *PROMOTIF* (Hutchinson & Thornton, 1996). The structure contains two domains: the lower portion is the cosubstrate-binding domain and the upper portion is the catalytic or substrate-binding domain. β-Strands are shown as green arrows and helices are shown in red. (*b*) The topology diagram generated with *TOPS* (http://www.tops.leeds.ac.uk) shows the two-domain enzyme, with the larger domain consisting of a seven-stranded β-sheet with Rossmann-fold topology that forms the cosubstrate-binding domain. The smaller domain is represented by a five-stranded β-sheet and forms the substrate-binding domain. Strands are depicted as green triangles and helices as red spheres. (*c*) View of the H(P)PR dimer approximately along the twofold rotation axis. The dimer interface is mainly composed of residues from the cosubstrate-binding domains.

drogenase, which contain a third domain, the so-called regulatory domain (Schuller *et al.*, 1995; Ha *et al.*, 2006, 2007). The smaller domain is known as the substrate-binding domain (Schuller *et al.*, 1995; Dengler *et al.*, 1997) or catalytic domain (Lamzin *et al.*, 1994; Goldberg *et al.*, 1994; Stoll *et al.*, 1996). The larger of the two domains is responsible for binding the cosubstrate and contains a conserved [G*X*G*XX*G(X_{17})D] motif that is characteristic of the NAD(P)H/NAD(P)$^+$-binding region. In the H(P)PR structure a serine residue (Ser174) is present at the position of the aspartate. The importance of this residue will be discussed in the context of cosubstrate binding. The two domains are connected by a two-stranded hinge. This hinge has been described as providing some flexibility to the domains during catalysis (Lamzin *et al.*, 1994; Schuller *et al.*, 1995; Stoll *et al.*, 1996).

According to the program *PROMOTIF* (Hutchinson & Thornton, 1996), the substrate-binding domain of H(P)PR consists of residues 2–100 and 285–313 and includes both termini (the upper domain in Fig. 3*a*). Sufficient electron density has not been observed for the first amino acid and the attached His tag, which suggests high flexibility of this part, as has frequently been observed in other crystal structures. The first 99 amino acids of the structure form a five-stranded parallel β-sheet flanked by five helices. Helices 3_{10}, α_2, α_3 and α_4 are located on the distal side of the β-sheet, whereas helix α_1 lies on the proximal side (Fig. 3*b*). The C-terminus runs parallel to helix α_1 on the proximal side and folds into a long helix (α_5). The general folding is very similar to the structures of D-glycerate dehydrogenase (Goldberg *et al.*, 1994) and glyoxylate reductase/hydroxypyruvate reductase (Booth *et al.*, 2006), with the difference that H(P)PR contains an additional 3_{10}-helix between β_2 and α_2.

The cosubstrate-binding domain consists of residues 101–284, forming a seven-stranded β-sheet (the lower domain in Fig. 3*a*). A total of six α-helices and four 3_{10}-helices flank this β-sheet. The topology corresponds to two Rossmann folds and is characteristic of the cosubstrate-binding domains in NAD(P)-dependent dehydrogenases. Compared with an ideal Rossmann fold, the helix between β_B and β_C is missing and two supplementary short 3_{10}-helices are inserted after β_D and β_E, respectively. Furthermore, one helix and one β-strand are inserted after β_F.

3.2. Dimer formation

H(P)PR forms a dimer in solution and in the crystal. In the latter, the dimer is formed by crystallographic symmetry (Fig. 3*c*). In the apo structure an average molecular surface area of 2141 Å^2 per monomer is buried, with 2025 Å^2 (94.5%) from the cosubstrate-binding domain, while only 116 Å^2 (5.5%) is from the catalytic domain. Molecular surfaces were calculated using the program *MS* (Connolly, 1983). The H(P)PR dimer interface is within the average range observed for homodimeric protein complexes of this size (Jones & Thornton, 1996). The described interface also shows a high shape complementarity (Sc), with an Sc of 0.75 as calculated using the program *SC* within *CCP*4 (Lawrence & Colman, 1993; Collaborative Computational Project, Number 4, 1994). Typically values range from 0.70 to 0.74 for oligomeric interfaces and from 0.71 to 0.76 for protein–protein inhibitor interfaces (Lawrence & Colman, 1993). Detailed analyses of the residues interacting in the dimer interface show that a total of 403 interactions are formed, with the majority (369) being van der Waals interactions. In addition, there are 28 hydrogen bonds and six salt bridges. From these observations it is concluded that the dimer is the biologically active form of H(P)PR. This is corroborated by the molecular mass determined for the native active H(P)PR by gel filtration, which was approximately twice the mass of the monomer after SDS–PAGE (Kim *et al.*, 2004).

3.3. Structure of H(P)PR complexed with NADP$^+$

After cocrystallization with the oxidized cosubstrate, the monomer of H(P)PR contained an NADP$^+$ molecule bound to the cosubstrate-binding domain, with a total of 16 hydrogen bonds to the main chain and side chains of ten amino-acid residues. In contrast to most D-2-hydroxyacid dehydrogenases for which structures have been published, H(P)PR prefers NADP(H) as cosubstrate. The preference of the enzyme for NADPH as a cofactor is reflected in the strongly different apparent K_m values for NADPH and NADH. Using pyruvate as the substrate, the K_m value for NADPH was measured to be 0.02 m*M*, while that for NADH was 0.5 m*M*. The amino acid responsible for discrimination between the two cosubstrates has been identified to be Asp175, which hinders the binding of the negatively charged phosphate group (Bernard *et al.*, 1994). Indeed, in the structures of D-lactate dehydrogenase (Razeto *et al.*, 2002), glycerate dehydrogenase (Goldberg *et al.*, 1994), formate dehydrogenase (Lamzin *et al.*, 1994), 3-phosphoglycerate dehydrogenase (Schuller *et al.*, 1995) and D-hydroxyisocaproate dehydrogenase (Dengler *et al.*, 1997) an Asp is present at the corresponding position. In contrast to these NAD(H)-dependent dehydrogenases, H(P)PR contains serine at this position (Ser174), allowing the binding of NADP(H). The phosphate group of the cosubstrate is fixed by five hydrogen bonds to neighbouring amino acids (Arg175 and Ser176) in H(P)PR. This strong binding and the positively charged environment may explain the preference for NADP(H) (Tanaka *et al.*, 1996). The recently published structure of human glyoxylate reductase/hydroxypyruvate reductase also shows the preferential use of NADP(H) and contains a glycine at the corresponding position (Gly184; Booth *et al.*, 2006).

Overall, the cosubstrate fits very well into the catalytic cleft of H(P)PR, similar to other enzymes of the family. The $F_o - F_c$ difference density of the cosubstrate is shown at the 3σ level in Fig. 4. The carboxamide group of the cosubstrate forms three hydrogen bonds to the protein (N41 to Asp256 OD2 and Ile230 O and O40 to His279 NE2), which result in a *cis* orientation with an angle of 31° to the pyridine plane. Similar angles have been reported for other structures [25° in formate dehydrogenase (Lamzin *et al.*, 1994) and 20° in D-lactate

dehydrogenase from *Lactobacillus bulgaricus* (Razeto *et al.*, 2002)].

The atomic temperature factor (or *B* factor) is defined by $B = 8\pi^2u^2$, where u is the mean atomic displacement and is highly correlated with the occupancy of the associated atom during crystallographic refinement. The average *B* factor for the cosubstrate is 29.6 Å^2. This suggests that the cosubstrate is fully occupied when compared with the average *B* factor for the protein atoms of 30.1 Å^2. Although different occupancies of the cosubstrate in the monomers have been reported for other enzymes (Booth *et al.*, 2006; Razeto *et al.*, 2002), there is only one monomer in the asymmetric unit in the H(P)PR structure and we assume equal occupancy in both monomers.

3.4. Domain movement

A movement of the two domains after cosubstrate binding in order to close the inter-domain cleft for catalysis has been reported for several D-isomer-specific 2-hydroxyacid dehydrogenases (Lamzin *et al.*, 1994; Booth *et al.*, 2006). Other authors have postulated that additional substrate binding is necessary for domain movement as the substrate stabilizes the closed conformation by supplementary hydrogen bonds (Razeto *et al.*, 2002). Nevertheless, taking into account that in a crystal lattice several contacts are made to the crystalline surroundings, cosubstrate binding alone could lead to a closed-conformation structure. The importance of the crystalline environment for the domain-opening angle was suggested by Dengler *et al.* (1997) for D-hydroxyisocaproate dehydrogenase, the structure which shows an open conformation even though both cosubstrate and substrate are bound.

In the H(P)PR structure no significant change in the domain-opening angle could be observed between the native and the NADP$^+$-complexed enzyme. The only recognizable change upon binding of the cosubstrate is a slight tilting movement of the substrate-binding domain in the direction of the proximal side of the protein. The resulting angle is 4.4°, with flexible regions at amino acids 100–101, 204–209 and 290–291, as calculated using the program *DYNDOM* (Hayward *et al.*, 1997; Hayward & Berendsen, 1998). Interestingly, this has little effect on the amino acids in the catalytic cleft. The regions taking part in this tilting movement are mainly the helices in the outer part of the catalytic domain.

Superposition of the H(P)PR structure with known structures of enzyme-family members indicates that the H(P)PR structures with and without bound cosubstrate are both in a closed conformation. The opening angle is similar to those of the holoenzymes of D-lactate dehydrogenase (Razeto *et al.*, 2002), formate dehydrogenase (Lamzin *et al.*, 1994) and glyoxylate reductase/hydroxypyruvate reductase (Booth *et al.*, 2006) (Fig. 5*a*).

To explain the closed conformation adopted in the apo structure, the domain interactions were investigated using the program *CONTACSYM* (Sheriff *et al.*, 1987) with domain partitioning as described above. In addition to several secondary hydrogen bonds mediated by water molecules, numerous direct interactions were calculated. 85 interactions (<4.33 Å) were identified in total and included 14 hydrogen bonds and one salt bridge after exact investigation of the density of the corresponding amino acids. Most of the contacts were observed in the region where the two domains contact each other.

The interactions in the catalytic cleft seem to be more significant. Here, three amino acids in each domain interact with the other domain, stabilizing the narrow cleft. The amino acids participating in the contacts are Leu205, Arg232 and His279 from the cosubstrate-binding domain and Ser53, Gly77 and Asp79 from the substrate-binding domain. These six amino acids are connected by seven van der Waals contacts, one short van der Waals contact (Ser53 CB to Arg232 NH_2, 3.2 Å) and one single salt bridge (Asp79 OD1 to Arg232 NE, 3.5 Å).

In the complex structure, these six amino acids show similar conformations. Comparable interactions are present in the holo structures of formate dehydrogenase (Lamzin *et al.*, 1994; complexed with NAD), D-lactate dehydrogenase (Razeto *et al.*, 2002; complexed with NADH) and glyoxylate reductase/hydroxypyruvate reductase (Booth *et al.*, 2006; complexed with NADPH) as Arg232, His279 and Gly77 are conserved amino acids in the enzyme family and Asp79 is also present in the above-mentioned structures. This suggests that the observed interactions between the two domains cannot be the only reason for the closed structure of apo H(P)PR. Nevertheless, these interactions might provide a stabilizing feature and together with the crystalline environment could lead to the observed closed conformation (Dengler *et al.*, 1997).

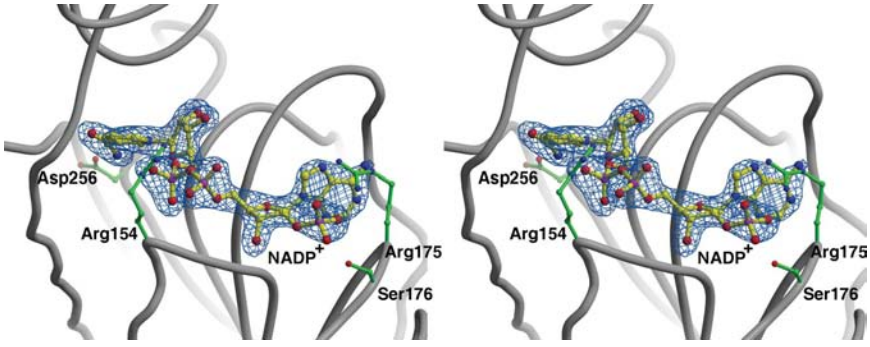

Figure 4
Stereoview of the cosubstrate (NADP$^+$) bound in the catalytic cleft of the complex structure. The $F_o - F_c$ density of the cosubstrate is shown at the 3σ level.

3.5. Catalytic site

The active site of H(P)PR is formed by the amino-acid residues Arg232 and His279. Furthermore, residue Glu261 forms a hydrogen bond (2.6 Å) to His279 and stabilizes His279, most likely in its protonated form. These catalytic residues are conserved in other dehydrogenases and

have been implicated in catalysis in D-2-hydroxyisocaproate dehydrogenase (Dengler *et al.*, 1997; Arg234, His295 and Glu263), D-glycerate dehydrogenase (Goldberg *et al.*, 1994; Arg240, His287 and Glu269) and D-lactate dehydrogenase (Razeto *et al.*, 2002; Arg235, His296 and Glu264). Two possible substrate-binding modes have been described to date for dehydrogenases (Goldberg *et al.*, 1994; Stoll *et al.*, 1996; Razeto *et al.*, 2002). Fig. 6 schematically shows pyruvate docked into the active site of H(P)PR. In binding mode *A* the carboxylate group of pyruvate forms hydrogen bonds of 2.7 and 3.1 Å (distances obtained from docking) to the amide backbone of Val76 and Gly77. Arg232 forms interactions with the carboxylate O atom (2.9 Å) and the carbonyl O atom (3.0 Å). This carbonyl O atom is further coordinated by His279 $N^{\delta2}$ (3.0 Å), which is held in position by Glu261, which forms a hydrogen bond to His279 $N^{\varepsilon1}$ (2.6 Å). The latter interaction is responsible for the protonated form of His279, which could then protonate the carbonyl functionality, thus better activating the carbonyl carbon for nucleophilic attack. Hydride transfer from NADPH would take place from below the plane, resulting in formation of the (*R*)-enantiomer. This model was predicted by Vinals *et al.* (1995) for D-lactate dehydrogenase derived from the formate dehydrogenase structure and was later used for D-lactate dehydrogenase (Stoll *et al.*, 1996; Razeto *et al.*, 2002) and D-2-hydroxyisocaproate dehydrogenase (Dengler *et al.*, 1997). Recently, Booth and coworkers showed that the substrate was clearly orientated this way in the structure of glyoxylate reductase/hydroxypyruvate dehydrogenase (Booth *et al.*, 2006).

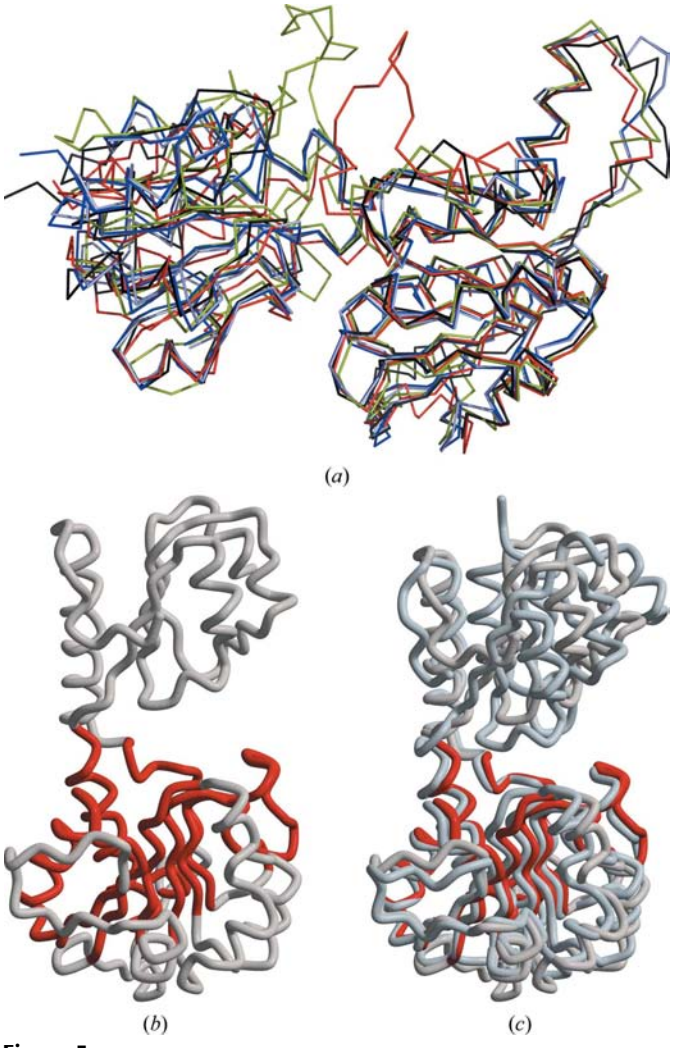

Figure 5
(*a*) Comparison of the opening angle between the substrate-binding and cosubstrate-binding domains. The native H(P)PR structure (PDB code 3ba1) is presented in dark blue, the H(P)PR complex structure (PDB code 3baz) in light blue, D-lactate dehydrogenase (PDB code 1j49, chain *B*) in red, formate dehydrogenase (PDB code 2nac) in green and glyoxylate reductase/hydroxypyruvate reductase (PDB code 2gcg) in black. (*b*) Homology model of H(P)PR depicted in grey. The model was generated from glycerate dehydrogenase, D-3-phosphoglycerate dehydrogenase and formate dehydrogenase with the *SWISS-MODEL* server. A 30% subset of the model shown in dark red was used for successful molecular replacement. (*c*) Superposition of the previous homology model on the final model of H(P)PR (shown in light blue). The H(P)PR structure has an r.m.s.d. of 2.6 Å to the model. The structure superimposes well on the lower cosubstrate-binding domain.

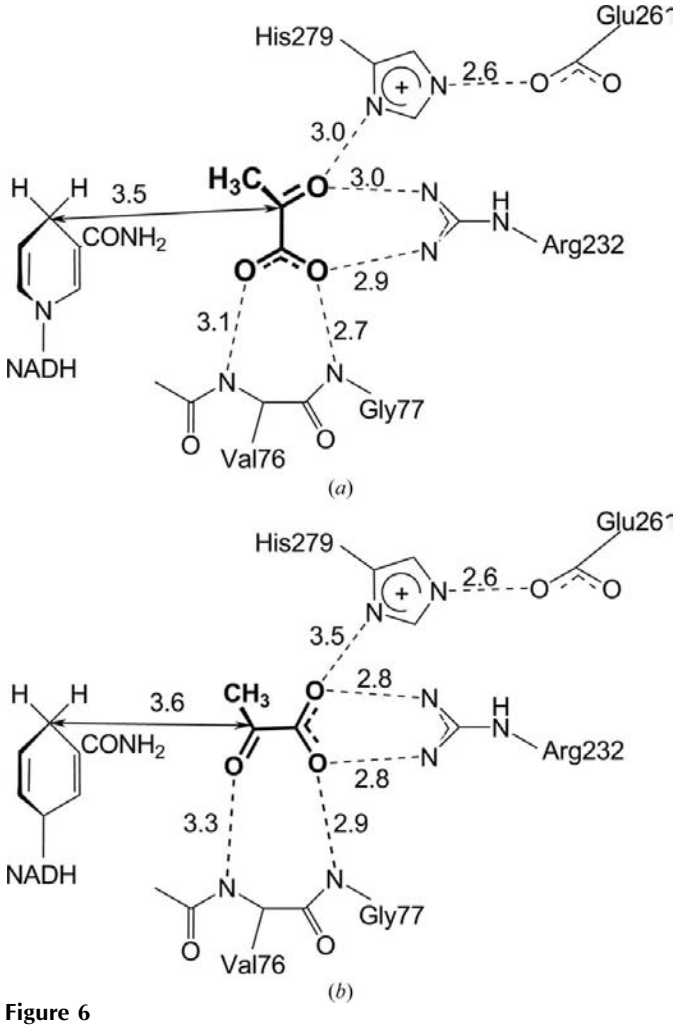

Figure 6
Two possible substrate-binding modes which have been described for dehydrogenases with pyruvate as substrate. (*a*) Mode *A*. The carboxylate group of pyruvate forms hydrogen bonds to the amide backbone of Val76 and Gly77, as well as to Arg232. The carbonyl O atom interacts with Arg232 and His279. (*b*) Mode *B*. The carboxyl group of pyruvate forms two hydrogen bonds to Arg232 and interacts with His279 and the backbone amide. The latter also bonds to the carbonyl group O atom.

The second binding mode (mode *B*) was suggested prior to mode *A* and was first used by Lamzin and coworkers for the substrate binding of formate in the formate dehydrogenase structure (Lamzin *et al.*, 1994). Goldberg and coworkers also used a similar orientation for D-glycerate dehydrogenase which was derived from the binding mode in L-lactate dehydrogenases (Goldberg *et al.*, 1994). In this second possible binding mode (mode *B*; Fig. 6*b*) the carboxyl group of pyruvate forms two hydrogen bonds to Arg232 (2.8 Å each). Here, both the carbonyl group O atom and the carboxyl group form hydrogen bonds to the backbone amide (3.3 and 2.9 Å, respectively). The carboxyl group is furthermore coordinated by His279, keeping it in the deprotonated form. Assuming this binding mode and hydride transfer from the cosubstrate from below the plane, the (*S*)-enantiomer would be formed. To further investigate these two binding modes, docking studies were performed with the substrates mentioned above.

3.6. Substrate docking

Structural comparison with other dehydrogenases revealed that the catalytic site of H(P)PR contained residues Val76, Gly77, Arg232, Glu261 and His279 [H(P)PR numbering]. All specific dehydrogenases contain corresponding conserved residues which form the core of the active site. The available crystal structures show the substrate to be located between these catalytic residues and the nicotinamide moiety of the cosubstrate.

In addition to the proposed natural substrate pHPP, several other possible substrates were tested for catalytic activity including DHPP, phenylpyruvate (PP), HP and pyruvate (P) (Fig. 2). Despite extensive efforts to obtain a ternary complex of H(P)PR with the bound cosubstrate $NADP^+$ and various substrates, none were obtained by cocrystallization or soaking experiments. The obtained electron density unambiguously showed incorporation of the cosubstrate but revealed only partial density at the possible substrate location. Therefore, all substrates were docked computationally into the active site using the program *AutoDock* (Morris *et al.*, 1998). This provides an initial insight into potential binding modes of the substrates at the catalytic site.

For each ligand, 100 positions were generated and the docking results were clustered and ranked according to their geometry and energy (Table 2). All five substrates mentioned above were docked into the binary protein–cosubstrate complex. Column 2 of Table 2 lists the cluster rank of the scored substrates and the corresponding cluster size. The majority of docking solutions were generally found within the first three clusters. These solutions adopted one of two possible binding modes termed *A* or *B* (*B** is a variation of binding mode *B*). These binding modes are depicted in Fig. 7. For each cluster the frequency of the docked binding mode, the top solution of each binding mode, the lowest docked energy and the stereochemistry of the corresponding products are listed. Since H(P)PR is D-isomer-specific, only the (*R*)-enantiomer was formed in the reaction. This was proven by analysis of the H(P)PR reaction product using chiral HPLC.

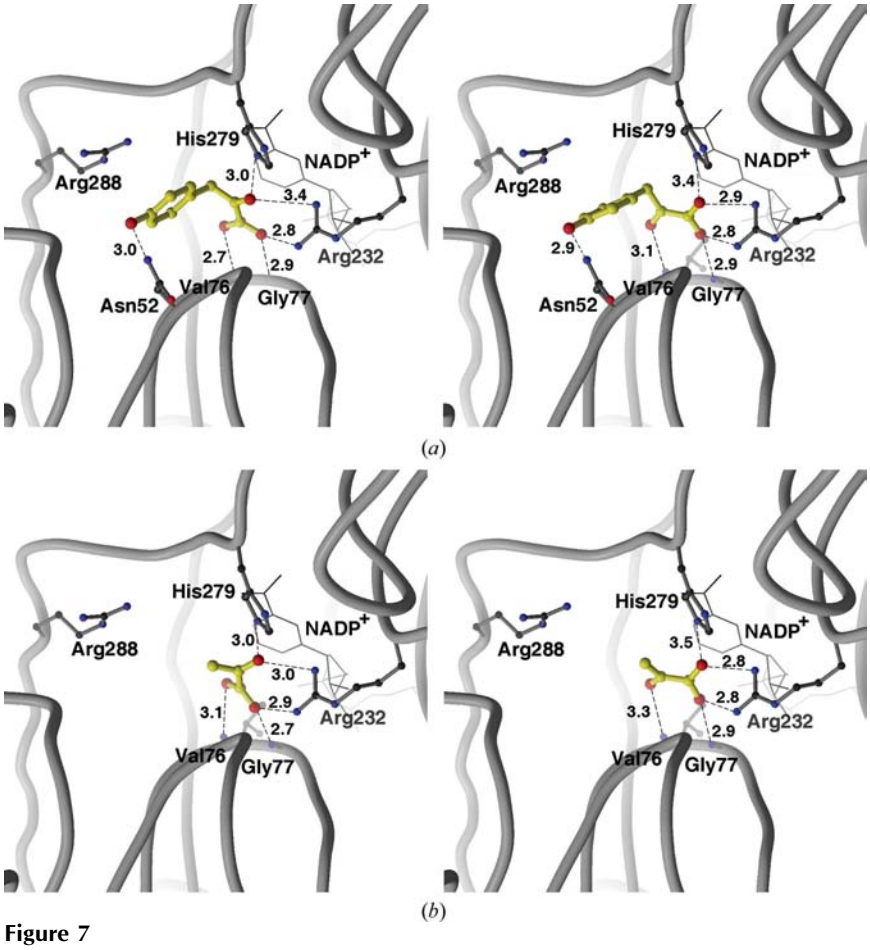

Figure 7
The two possible binding modes resulting from docking with *AutoDock*. (*a*) Binding modes for pHPP, with binding mode *A* on the left and binding mode *B* on the right. For large substrates both binding modes were found nearly equally. (*b*) The two pictures visualize the two docking modes for pyruvate. For pyruvate, binding mode *A* (picture on the left) was clearly favoured.

For the putative natural substrate pHPP the top cluster contained 95 docking poses, with 57 showing binding mode *B* and 38 binding mode *A*. Interestingly, the lowest docked energy of -39.31 kJ mol^{-1} was found for binding mode *B*, which would result in formation of the (*S*)-enantiomer. However, the energy difference between mode *B* and mode *A* (-39.14 kJ mol^{-1}) of 0.17 kJ mol^{-1} was minimal. For DHPP, PP and HP the top solution was found for binding mode *A*, but again with only a very small energy gap from binding mode *B*. For pyruvate the top solution was found for binding mode *A* with high frequency and a large cluster size and here the energy difference from the next small cluster with binding mode *B* was more significant.

Table 2
Overview of docking results.

pHPP, 4-hydroxyphenylpyruvate; DHPP, 3,4-dihydroxyphenylpyruvate; PP, phenylpyruvate; HP, hydroxypyruvate; P, pyruvate.

Substrate	Cluster rank/size	Lowest docked energy (kJ mol^{-1})	Binding mode	Frequency of binding mode	Stereochemistry
pHPP	1/95	−39.31	*B*	57	*S*
		−39.14	*A*	38	*R*
	2/3	−37.30	*B**	3	*R*
DHPP	1/7	−41.53	*A*	6	*R*
	2/42	−41.32	*B*	38	*S*
		−40.10	*A*	4	*R*
	3/33	−40.31	*A*	32	*R*
		−38.89	*B*	1	*S*
	4/6	−40.14	*A*	6	*R*
PP	1/95	−37.21	*A*	49	*R*
		−37.13	*B*	46	*S*
	2/5	−37.00	*B*	5	*S*
HP	1/60	−27.13	*A*	48	*R*
		−26.62	*B*	12	*S*
	2/29	−26.79	*A*	18	*R*
		−26.41	*B*	11	*S*
	3/8	−26.20	*B**	8	*R*, *S*
P	1/97	−24.74	*A*	90	*R*
		−24.07	*B*	7	*S*
	2/3	−23.86	*B**	3	*R*

In conclusion, modelling of the substrates shows two possible binding modes with approximately the same energy of binding. Both binding modes are contained in the top clusters, which are highly populated. The docking of substrates does not allow the exclusion of one binding mode. While hydride transfer from the cosubstrate from below the plane to the carbonyl O atom in both binding modes depicted in Figs. 6(*a*) and 6(*b*) seems reasonable, the protonation of the carbonyl O atom also has to be considered. Following the substrate orientation in binding mode *B*, in which the carbonyl O atom forms a hydrogen bond to the backbone amide of Val76, protonation through this interaction is unlikely. In contrast, in binding mode *A* the carbonyl O atom forms hydrogen bonds to His279 and Arg232, both of which are capable of donating a proton. Since this results in the (*R*)-enantiomer of pHPL, formation of the (*S*)-enantiomer can be excluded.

4. Conclusions

H(P)PR is an enzyme that is involved in the biosynthesis of rosmarinic acid, which has antibacterial, antiviral and antioxidant properties. We determined the crystal structure of a D-isomer-specific 2-hydroxyacid dehydrogenase with HPPR activity from the higher plant *C. blumei* at 1.47 Å resolution. The overall structure shows the characteristic two-domain arrangement observed for this enzyme family. The smaller of the two domains is responsible for substrate binding, whereas the larger domain binds the cosubstrate. The catalytic cleft is located between the two domains. Surprisingly, the complex structure with NADP$^+$ determined at 2.2 Å resolution shows no significant change in the domain-opening angle as was previously observed for similar enzymes upon complex formation. H(P)PR is active as a dimer and dimer formation could be demonstrated in the crystal structure.

In addition to 4-hydroxyphenylpyruvate, the enzyme also accepts substrates such as 3,4-dihydroxyphenylpyruvate and hydroxypyruvate. The catalytic site of the enzyme consists of the conserved residues Arg232, His279 and Glu261. Docking studies with substrates revealed two possible binding modes, termed *A* and *B*, with similar docking energy. However, only binding mode *A* provides the necessary environment in the active centre for hydride and proton transfer during reduction, leading to the formation of the (*R*)-enantiomer of lactate and/or hydroxyphenyllactate.

We are most grateful to Dr Klaus Reuter for his support in the crystallization of the native protein and Dr Holger Steuber for his helpful advice during data refinement. Furthermore, we thank Christian Sohn for his assistance during crystallization and data collection with the Rigaku copper rotating-anode generator and the support staff at BESSY II, Berlin for their help with the synchrotron data collection. We thank the Bundesministerium für Bildung und Forschung (05 ES3XBA/5) for financing the travel costs to BESSY II.

References

Arévalo, J. H., Stura, E. A., Taussig, M. J. & Wilson, I. A. (1993). *J. Mol. Biol.* **231**, 103–118.
Bernard, N., Johnsen, K., Ferain, T., Garmyn, D., Hols, P., Holbrook, J. J. & Delcour, J. (1994). *Eur. J. Biochem.* **224**, 439–446.
Bonete, M., Ferrer, J., Pire, C., Penades, M. & Ruiz, J. (2000). *Biochimie*, **82**, 1143–1150.
Booth, M. P. S., Conners, R., Rumsby, G. & Brady, R. L. (2006). *J. Mol. Biol.* **360**, 178–189.
Brünger, A. T., Adams, P. D., Clore, G. M., DeLano, W. L., Gros, P., Grosse-Kunstleve, R. W., Jiang, J.-S., Kuszewski, J., Nilges, M., Pannu, N. S., Read, R. J., Rice, L. M., Simonson, T. & Warren, G. L. (1998). *Acta Cryst.* D**54**, 905–921.
Bugg, T. D., Wright, G. D., Dutka-Malen, S., Arthur, M., Courvalin, P. & Walsh, C. T. (1991). *Biochemistry*, **30**, 10408–10415.
Case, D. A. *et al.* (2006). *AMBER* 9. University of California, San Francisco. http://ambermd.org/.
Collaborative Computational Project, Number 4 (1994). *Acta Cryst.* D**50**, 760–763.
Connolly, M. L. (1983). *J. Appl. Cryst.* **16**, 548–558.
Dengler, U., Niefind, K., Kiess, M. & Schomburg, D. (1997). *J. Mol. Biol.* **267**, 640–660.
Gasteiger, J. & Marsili, M. (1980). *Tetrahedron*, **36**, 3219–3228.
Goldberg, J. D., Yoshida, T. & Brick, P. (1994). *J. Mol. Biol.* **236**, 1123–1140.
Grant, G. A. (1989). *Biochem. Biophys. Res. Commun.* **165**, 1371–1374.
Greenler, J. M., Sloan, J. S., Schwartz, B. W. & Becker, W. M. (1989). *Plant Mol. Biol.* **13**, 139–150.
Ha, J. Y., Lee, J. H., Kim, K. H., Kim, D. J., Lee, H. H., Kim, H.-K., Yoon, H.-J. & Suh, S. W. (2006). *Acta Cryst.* F**62**, 139–141.
Ha, J. Y., Lee, J. H., Kim, K. H., Kim, D. J., Lee, H. H., Kim, H.-K., Yoon, H.-J. & Suh, S. W. (2007). *J. Mol. Biol.* **366**, 1294–1304.
Häusler, E., Petersen, M. & Alfermann, A. W. (1991). *Z. Naturforsch. C*, **46**, 371–376.
Hayward, S. & Berendsen, H. J. (1998). *Proteins*, **30**, 144–154.
Hayward, S., Kitao, A. & Berendsen, H. J. (1997). *Proteins*, **27**, 425–437.

Hutchinson, E. G. & Thornton, J. M. (1996). *Protein Sci.* **5**, 212–220.
Jones, S. & Thornton, J. M. (1996). *Proc. Natl Acad. Sci. USA*, **93**, 13–20.
Jones, T. A., Zou, J.-Y., Cowan, S. W. & Kjeldgaard, M. (1991). *Acta Cryst.* A**47**, 110–119.
Julliard, J. H. & Breton-Gilet, A. (1997). *Protein Expr. Purif.* **9**, 10–14.
Kim, K. H., Janiak, V. & Petersen, M. (2004). *Plant Mol. Biol.* **54**, 311–323.
Kleczkowski, L. A., Givan, C. V., Hodgson, J. M. & Randall, D. D. (1988). *Plant Physiol.* **88**, 1182–1185.
Lamzin, V. S., Dauter, Z., Popov, V. O., Harutyunyan, E. H. & Wilson, K. S. (1994). *J. Mol. Biol.* **236**, 759–785.
Lamzin, V. S. & Wilson, K. S. (1993). *Acta Cryst.* D**49**, 129–147.
Lawrence, M. C. & Colman, P. M. (1993). *J. Mol. Biol.* **234**, 946–950.
McCoy, A. J., Grosse-Kunstleve, R. W., Storoni, L. C. & Read, R. J. (2005). *Acta Cryst.* D**61**, 458–464.
Moews, P. C. & Kretsinger, R. H. (1975). *J. Mol. Biol.* **91**, 229–232.
Morris, G. M., Goodsell, D. S., Halliday, R. S., Huey, R., Hart, W. E., Belew, R. K. & Olson, A. J. (1998). *J. Comput. Chem.* **19**, 1632–1662.
Navaza, J. (1994). *Acta Cryst.* A**50**, 157–163.
Nessler, S., Le Bras, G., Le Bras, G. & Garel, J. R. (1994). *J. Mol. Biol.* **235**, 370–371.
Nunez, M. F., Pellicer, M. T., Badia, J., Aguilar, J. & Baldoma, L. (2001). *Biochem. J.* **354**, 707–715.
Otwinowski, Z. & Minor, W. (1997). *Methods Enzymol.* **276**, 307–326.
Petersen, M. & Alfermann, A. W. (1988). *Z. Naturforsch. C*, **43**, 501–504.
Petersen, M., Häusler, E., Karwatzki, B. & Meinhard, J. (1993). *Planta*, **189**, 10–14.
Razeto, A., Kochhar, S., Hottinger, H., Dauter, M., Wilson, K. S. & Lamzin, V. S. (2002). *J. Mol. Biol.* **318**, 109–119.
Read, R. J. (2001). *Acta Cryst.* D**57**, 1373–1382.
Schuller, D. J., Grant, G. A. & Banaszak, L. J. (1995). *Nature Struct. Biol.* **2**, 69–76.
Schwede, T., Kopp, J., Guex, N. & Peitsch, M. C. (2003). *Nucleic Acids Res.* **31**, 3381–3385.
Sheldrick, G. M. (2008). *Acta Cryst.* A**64**, 112–122.
Sheriff, S., Hendrickson, W. A. & Smith, J. L. (1987). *J. Mol. Biol.* **197**, 273–296.
Stoll, V. S., Kimber, M. S. & Pai, E. F. (1996). *Structure*, **4**, 437–447.
Tanaka, N., Nonaka, T., Nakanishi, M., Deyashiki, Y., Hara, A. & Mitsui, Y. (1996). *Structure*, **4**, 33–45.
Timm, S., Nunes-Nesi, A., Pärnik, T., Morgenthal, K., Wienkoop, S., Keerberg, O., Weckwerth, W., Kleczkowski, L. A., Fernie, A. R. & Bauwe, H. (2008). *Plant Cell*, **20**, 2848–2859.
Vagin, A. & Teplyakov, A. (1997). *J. Appl. Cryst.* **30**, 1022–1025.
Vinals, C., De Bolle, X., Depiereux, E. & Feytmans, E. (1995). *Proteins*, **21**, 307–318.
Yum, D. Y., Lee, B. Y., Hahm, D. H. & Pan, J. G. (1998). *J. Bacteriol.* **180**, 5984–5988.